TORSIONAL RESPONSE OF HORIZONTALLY CURVED BRIDGES SUBJECTED TO EARTHQUAKE-INDUCED POUNDING

M. Amjadian [(1)], A. K. Agrawal [(2)]

[(1)] *PhD Candidate, The City College of the City University of New York, mamjadian@ccny.cuny.edu.*
[(2)] *Professor, The City College of the City University of New York, agrawal@ccny.cuny.edu.*

Abstract

Horizontally curved bridges have been observed to be highly vulnerable to severe seismic damage, such as deck unseating, because of the strong tendency of their decks to in-plane rotation. The torsional demand of these bridges may dramatically increases when they are subjected to earthquake-induced pounding, as observed in Baihua and Huilan bridges during 2008 Wenchuan earthquake in China. This paper is focused on studying the influence of seismic pounding, deck-abutment collision, on the torsional response of horizontally curved bridges in strong earthquakes. For this purposes, a three-degree-of-freedom nonlinear model has been developed to capture key dynamic parameters affecting the seismic response of these types of bridges. In the model, the radial and azimuthal shear-displacement relations of the columns and their bilateral interactions are modeled by a coupled-biaxial bilinear hysteresis spring, but their torsional moment-rotation relations are molded by a linear spring; and the normal and tangential impact forces at the contact nodes between the deck and the abutments are modeled by Jankowski contact model and Karnopp friction model, respectively. Then, the nonlinear bridge model is utilized to perform a detailed parametric analysis on the torsional response of a prototype curved bridge based on variations of these key parameters of the model: (i) subtended angle of the deck, β; (ii) size of the gap between the deck and the abutments, δ_g; (iii) normalized static radial stiffness eccentricity, η_{sr}. The results obtained from this numerical analysis indicate that the seismic pounding has a noticeable effect on the in-plane rotation of the curved bridge deck particularly when the distance between the stiffness center and the curvature center of the deck is increased.

Keywords: Horizontally Curved Bridge; Seismic Pounding; Torsional Response; Non-Linear Model; Parametric Analysis.

1. Introduction

In the recent decades, horizontally curved bridges have been widely used in urban transportation networks around the world. The curved geometries of these bridges enable them to be suitably located in complex grade-separated intersections and interchanges where there is a strong emphasis on aesthetic and space-compatible structural designs at the same time [1,2]. However, due to their irregular geometries and asymmetric stiffness and non-uniform mass distributions, horizontally curved bridges, similar to other types of irregular bridges such as skew bridges [3–5], are more susceptible to seismic failure than straight bridges [6–8]. It is also believed that multi-support irregular bridges, such as skew and curved bridges, are more susceptible to the rotational components of strong ground motions [9,10]. The unique structural features, inherent in horizontally curved bridges, have significant impacts on the amplification of the torsional response of the decks of these bridges particularly when they collide with the abutments during strong earthquakes (i.e. earthquake-induced pounding). The impact forces resulted from the collision will likely cause large radial and azimuthal displacements in the bearings at the abutments, and consequently, unseating of the decks from the abutments [1]. For example, it has been reported that seismic pounding was an effective factor in structural failures of Baihua and Huilan bridges during 2008 Wenchuan earthquake in China with a high moment magnitude of M_W=7.9 [11–13].

A large number of horizontally curved bridges either collapsed or suffered serious damage in the great 1971 San Fernando earthquake in California [7]; and since then, the vulnerability of these bridges to seismic damage has been a subject of interest to many researchers. However, there have been few studies on the vulnerability of horizontally curved bridges to earthquake-induced pounding. Williams and Godden [14] conducted an experimental study on the seismic response of a small scale model of a curved RC bridge that suffered extensive damage during the 1971 San Fernando earthquake. The authors considered the effects of sliding and seismic pounding at the expansion joints and ductility in the columns. Ijima et al. [15] used analytical and experimental models to study the influence of seismic pounding on the collapse of the decks of skew and curved bridges. The study was inspired by observation of the deck unseating in these bridges because of seismic pounding in the 1995 Kobe earthquake in Japan. Wieser et al. [16] performed an experimental test on a 2/5 scale model to investigate the effects of deck-abutment collision on the overall seismic performance of horizontally curved bridges. Ruiz Julian et al. [17] studied the efficiency of cable restrainers in the protection of curved steel viaducts from deck unseating caused by seismic pounding. Recently, Amjadian and Agrawal [1] have carried out an extensive parametric study on the influence of seismic pounding on the rigid-body motion of horizontally symmetric curved bridges.

This paper, using a three-degree-of-freedom nonlinear model, studies the sensitivity of the torsional response of horizontally one-way-asymmetric curved bridges to earthquake-induced pounding. The model is based on a recent work of the authors conducted to study the rigid-body motion of horizontally symmetric curved bridges subjected to earthquake-induced pounding. [1]. In this paper, this model has been employed to perform a detailed parametric analysis to particularly study the influence of different parameters on the torsional response of a prototype curved bridge affected by seismic pounding.

2. Mathematical Modeling of the Problem

The curved geometry of the deck of a horizontally curved bridge diverts the direction of the reaction forces of the columns from the principal axes of the bridge during an earthquake excitation that couples the torsional motion of the deck to its translational motions. This coupled motion may impose much worse condition on the motion of the deck when it is associated with seismic pounding between the deck and the abutments. Fig. 1 shows the dynamic model used to deal with such features inherent in the dynamic behavior of horizontally curved bridges [1]. This model is valid under these basic assumptions: (i) the deck is rigid [3,4,18,19]; (ii) the soil-structure interaction is negligible [20]; (iii) the bearings used at the abutments act as ideal roller supports; (iv) the mass of the bridge is entirely attributed to the mass center of the deck [21]; and (v) the shear-displacement relations of the columns are bilinear but their torsional moment-rotation relations are linear.

2.1 Dynamic model

The general geometrical features of the proposed dynamic model are shown in Fig. 1. The in-plane rigid-body motion of the deck subjected to earthquake-induced pounding is formulated in the xy-coordinate system. However, the restoring forces of the columns and the impact forces between the deck and the abutments are described in the rϕ- and nt-coordinate systems, respectively, as shown in Fig. 1. The curved geometry of the deck is idealized by a circular arc represented by subtended angle β ($0<\beta<\pi$), radius R and width W. It is assumed that the curvature center of the deck is coincident with the origin of the xy- and rϕ-coordinate systems (i.e. point O(0,0)). The degrees of freedom of the model, u_{ox}, u_{oy}, and θ, are assigned to this point. The y-axis is the axis of symmetry of the deck. The mass center of the deck, $C_m(0,y_m)$, is located on this axis. The polar coordinate of *i*-th column is $C_{si}(r_{si},\phi_{si})$ in which angle ϕ_{si} is bounded in the interval $|\phi_{si}-\pi/2|<\beta/2$ [1]. The restoring forces of *i*-th column is modeled with two bilinear translational springs with radial and azimuthal initial stiffnesses k_{sri} and $k_{s\phi i}$, post- to pre-yield stiffness ratios α_{sri} and $\alpha_{s\phi i}$, and yield displacements d_{ysri} and $d_{ys\phi i}$, receptively, and a linear rotational spring with stiffness $k_{s\theta i}$.

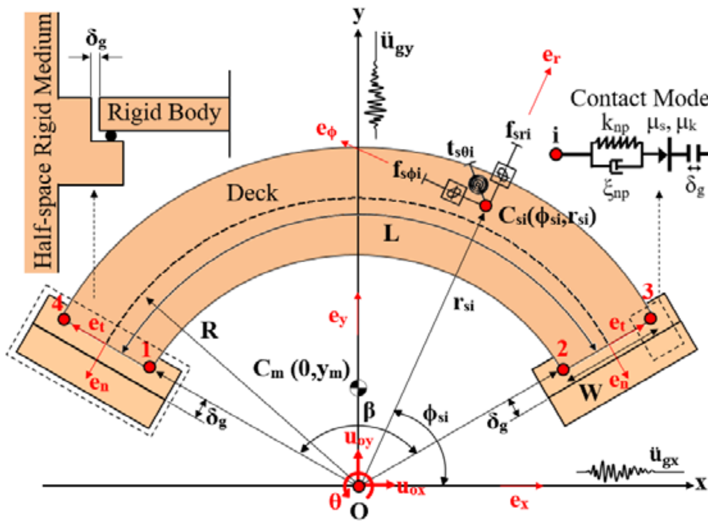

Fig. 1 – 3DOF dynamic model of typical horizontally curved bridges

The y-coordinate of the mass center, y_m, and the radius of gyration of the deck about the curvature center, r_o, can be respectively calculated by the following expressions [1],

$$y_m = \left(2+\frac{1}{6}\frac{\beta^2}{\nu^2}\right)\frac{\sin\frac{\beta}{2}}{\beta}R \quad , \quad r_o = \left(1+\frac{1}{4}\frac{\beta^2}{\nu^2}\right)^{\frac{1}{2}} \tag{1}$$

where υ=L/W is aspect ratio of the deck (υ>1).

2.2 Restoring forces of columns

The restoring force vector of *i*-th column represented in the rϕ-coordinate system is $\mathbf{F}_{si}=\{f_{sri}, f_{s\phi i}, t_{s\theta i}\}^T$. The radial, f_{sri}, and azimuthal, $f_{s\phi i}$, shear forces and their interactions during the earthquake excitation are modeled by the normalized form of Wang-Wen biaxial hysteresis model by disregarding its strength reduction effects [22]. However, for the sake of simplicity, the torsional moment, $t_{s\theta i}$, is modeled by a linear spring. The effect of the natural damping is disregarded; it will be taken into account later when the equation of motion of the bridge is developed. Therefore, $\mathbf{F}_{si}$ is given by [1],

$$\mathbf{F}_{si}(t) = \mathbf{K}_{si}\mathbf{U}_{si}(t) + \mathbf{H}_{si}(t) \tag{2}$$

where $\mathbf{K}_{si}$=Diag($\alpha_{sri}k_{sri}$, $\alpha_{s\phi i}k_{s\phi i}$, $k_{s\theta i}$) is post-yielding stiffness matrix, $\mathbf{U}_{si}(t)=\{u_{sri}, u_{s\phi i}, \theta\}^T$ is deflection vector, and $\mathbf{H}_{si}(t)=\{h_{sri}, h_{s\phi i}, 0\}^T$ is hysteresis force vector in which $h_{sri}=(1-\alpha_{sri})f_{ysri}z_{sri}$ and $h_{s\phi i}=(1-\alpha_{s\phi i})f_{ys\phi i}z_{s\phi i}$ where f_{ysri} and $f_{ys\phi i}$ are radial and azimuthal yield forces; z_{sri} and $z_{s\phi i}$ are dimensionless hysteresis variables given by the following coupled nonlinear first-order differential equations [22],

$$\begin{aligned}
\dot{z}_{sri} &= \frac{1}{d_{ysri}}\Big[A_s\dot{u}_{sri} - \Big(|\dot{u}_{sri}||z_{sri}|^{n-1}[\beta_s + \gamma_s \mathrm{sgn}(\dot{u}_{sri}z_{sri})] + |\dot{u}_{s\phi i}||z_{s\phi i}|^{n-1}[\beta_s + \gamma_s \mathrm{sgn}(\dot{u}_{s\phi i}z_{s\phi i})]\eta_s\Big)z_{sri}\Big] \\
\dot{z}_{s\phi i} &= \frac{1}{d_{ys\phi i}}\Big[A_s\dot{u}_{s\phi i} - \Big(|\dot{u}_{s\phi i}||z_{s\phi i}|^{n-1}[\beta_s + \gamma_s \mathrm{sgn}(\dot{u}_{s\phi i}z_{s\phi i})] + |\dot{u}_{sri}||z_{sri}|^{n-1}[\beta_s + \gamma_s \mathrm{sgn}(\dot{u}_{sri}z_{sri})]\eta_s\Big)z_{s\phi i}\Big]
\end{aligned} \tag{3}$$

In Eq. (3), {A_s, n, γ_s, β_s} are parameters that control the shape and the size of the hysteretic loop, η_s represents the biaxial interaction between the radial and azimuthal shear forces, and sgn(.) represents signum function. These parameters are selected in such a way that they represent an ideal bilinear hysteresis model with a biaxial coupled behavior along the r- and ϕ-axes [1]: A_s=1, n=25, $\gamma_s=\beta_s$=0.5, and η_s=1.

2.3 Impact forces

The normal impact forces between the deck and the abutments are modeled by nonlinear viscoelastic model, known as Jankowski contact model [23,24]. This model consists of a nonlinear spring in parallel with a nonlinear damper to simulate the kinetic energy absorption and dissipation, respectively. The damping part only acts during the approach phase of collision, and consequently, most of the energy is dissipated in this phase. The amount of energy dissipated during the restitution phase is negligible. Furthermore, the tangential impact force (i.e. friction force) is modeled by Karnopp friction model [1,25], considering the effects of stick-slip phenomenon at the contact nodes. It is assumed that the collisions between the deck and the abutments occur at the corners of the deck denoted as #1, #2, #3, and #4 in Fig. 1. The contact forces at the left side for *i*-th (i=1 and 4) contact node are,

$$\begin{gathered}
f_{pnli}(t) = \begin{cases} k_{pn}\delta_{pnli}(t)^{3/2} + c_{pnli}\dot{\delta}_{pnli}(t) & \delta_{pnli}(t) > 0 \quad \dot{\delta}_{pnli}(t) > 0 \\ k_{pn}\delta_{pnli}(t)^{3/2} & \delta_{pnli}(t) > 0 \quad \dot{\delta}_{pnli}(t) \le 0 \\ 0 & \delta_{pnli}(t) \le 0 \end{cases} \\
c_{pnli} = 2\xi_{pn}\sqrt{Mk_{pn}\sqrt{\delta_{pnli}(t)}} \quad , \quad \delta_{pnli}(t) = \mathbf{N}_{pli}^T\mathbf{U}_o(t) - \delta_g \quad , \quad \dot{\delta}_{pnli}(t) = \mathbf{N}_{pli}^T\dot{\mathbf{U}}_o(t) \\
f_{ptli}(t) = \begin{cases} \mu_k f_{pnli}(t)\mathrm{sgn}(\dot{\delta}_{ptli}) & |\dot{\delta}_{ptli}| \ge v_{s0} \\ f_{etli}(t) & |\dot{\delta}_{ptli}| < v_{s0} \quad \mu_s f_{pnli}(t) > |f_{etli}| \\ \mu_s f_{pnli}(t)\mathrm{sgn}(f_{etli}) & |\dot{\delta}_{ptli}| < v_{s0} \quad \mu_s f_{pnli}(t) \le |f_{etli}| \end{cases} \quad , \quad \dot{\delta}_{ptli}(t) = \mathbf{T}_{pli}^T\dot{\mathbf{U}}_o(t)
\end{gathered} \tag{4}$$

in which $\mathbf{N}_{pli}=\{-\cos(\beta/2), -\sin(\beta/2), r_{pli}\}^T$, $\mathbf{T}_{pli}=\{-\sin(\beta/2), +\cos(\beta/2), 0\}^T$, r_{pl1}=R-W/2, and r_{pl4}=R+W/2. The contact forces at the right side for *i*-th (i=2 and 3) contact node are,

$$f_{pnri}(t)=\begin{cases} k_{pn}\delta_{pnri}(t)^{3/2}+c_{pnri}\dot{\delta}_{pnri}(t) & \delta_{pnri}(t)>0 \quad \dot{\delta}_{pnri}(t)>0 \\ k_{pn}\delta_{pnri}(t)^{3/2} & \delta_{pnri}(t)>0 \quad \dot{\delta}_{pnri}(t)\le 0 \\ 0 & \delta_{pnri}(t)\le 0 \end{cases}$$

$$c_{pnri}=2\xi_{pn}\sqrt{Mk_{pn}\sqrt{\delta_{pnri}(t)}} \quad , \quad \delta_{pnri}(t)=-\mathbf{N}_{pri}^{T}\mathbf{U}_{o}(t)-\delta_{g} \quad , \quad \dot{\delta}_{pnri}(t)=-\mathbf{N}_{pri}^{T}\dot{\mathbf{U}}_{o}(t) \tag{5}$$

$$f_{ptri}(t)=\begin{cases} \mu_{k}f_{pnri}(t)\mathrm{sgn}(\dot{\delta}_{ptri}) & \left|\dot{\delta}_{ptri}\right|\ge v_{s0} \\ f_{etri}(t) & \left|\dot{\delta}_{ptri}\right|<v_{s0} \quad \mu_{s}f_{pnri}(t)>\left|f_{etri}\right| \\ \mu_{s}f_{pnri}(t)\mathrm{sgn}(f_{etri}) & \left|\dot{\delta}_{ptri}\right|<v_{s0} \quad \mu_{s}f_{pnri}(t)\le\left|f_{etri}\right| \end{cases} \quad , \quad \dot{\delta}_{ptri}(t)=\mathbf{T}_{pri}^{T}\dot{\mathbf{U}}_{o}(t)$$

in which $\mathbf{N}_{pri}=\{-\cos(\beta/2), +\sin(\beta/2), r_{pri}\}^T$ and $\mathbf{T}_{pri}=\{+\sin(\beta/2), +\cos(\beta/2), 0\}^T$, r_{pr2}=R-W/2, and r_{pr3}=R+W/2.

In Eqs. (4) and (5), $\delta_{pnai}(t)$ and $\delta_{ptai}(t)$ are relative normal and tangential displacements at the contact nodes, $\dot{\delta}_{pnai}(t)$ and $\dot{\delta}_{ptai}(t)$ are relative normal and tangential velocities at the contact nodes (subscript "a" is associated with the abutment number, i.e. on left side: {a≡l; i=1, 4} and on right side: {a≡r; i=2, 3}), δ_g is the size of the gap, k_{pn} is impact stiffness parameter, and ξ_{pn} is damping ratio. In the friction model, μ_s and μ_k are static and kinetic coefficients of friction, respectively, v_{s0} is a velocity limit with a small value below which the velocity of the contact node is assumed to be zero when the contact node sticks, and $f_{etai}(t)$ is the external force acting upon the deck at the contact node during the sticking phase, i.e. $\ddot{\delta}_{ptai}(t)=0$. The force will be formulated in section 2.4.

2.4 Equation of motion

The equation of motion of the bridge is given by [1],

$$\mathbf{M}\ddot{\mathbf{U}}_{o}(t)+\mathbf{C}\dot{\mathbf{U}}_{o}(t)+\mathbf{K}\mathbf{U}_{o}(t)+\mathbf{H}_{s}(t)+\mathbf{F}_{p}(t)=-\mathbf{M}\ddot{\mathbf{U}}_{g}(t) \tag{6}$$

where $\mathbf{U}_{o}(t)=\{u_{ox},u_{oy},\theta\}^{T}$, $\dot{\mathbf{U}}_{o}(t)=\{\dot{u}_{ox},\dot{u}_{oy},\dot{\theta}\}^{T}$, and $\ddot{\mathbf{U}}_{o}(t)=\{\ddot{u}_{ox},\ddot{u}_{oy},\ddot{\theta}\}^{T}$ are relative displacement, velocity and acceleration vectors of the curvature center of the deck, respectively, and $\ddot{\mathbf{U}}_{g}(t)=\{\ddot{u}_{gx},\ddot{u}_{gy},0\}^{T}$ is ground acceleration vector. The rest of matrices and vectors used in this equation are defined as follows:

i) **M** is mass matrix of the bridge defined as,

$$\mathbf{M}=\begin{bmatrix} M & 0 & -My_{m} \\ 0 & M & 0 \\ -My_{m} & 0 & I_{o} \end{bmatrix} \tag{7}$$

where M is the total mass of the deck.

ii) **K** is post-yielding stiffness matrix of the bridge given as,

$$\mathbf{K}=\begin{bmatrix} K_{XX} & K_{XY} & -K_{\Phi}r_{s}\sin\phi_{s} \\ K_{XY} & K_{YY} & +K_{\Phi}r_{s}\cos\phi_{s} \\ -K_{\Phi}r_{s}\sin\phi_{s} & +K_{\Phi}r_{s}\cos\phi_{s} & K_{\Theta}+r_{s}^{2}K_{\Phi} \end{bmatrix} \tag{8}$$

where K_{XX}, K_{XY}, K_{YY}, K_{Φ}, and K_{Θ} are defined as [1],

$$K_{XX} = \sum_{i=1}^{n_s}\left[\alpha_{sri}k_{sri}\cos^2\phi_{si} + \alpha_{s\phi i}k_{s\phi i}\sin^2\phi_{si}\right]$$
$$K_{XY} = \sum_{i=1}^{n_s}\left[(\alpha_{sri}k_{sri} - \alpha_{s\phi i}k_{s\phi i})\sin\phi_{si}\cos\phi_{si}\right]$$
$$K_{YY} = \sum_{i=1}^{n_s}\left[\alpha_{sri}k_{sri}\sin^2\phi_{si} + \alpha_{s\phi i}k_{s\phi i}\cos^2\phi_{si}\right] \tag{9}$$
$$K_{\Phi} = \sum_{i=1}^{n_s}\left[\alpha_{s\phi i}k_{s\phi i}\right]$$
$$K_{\Theta} = \sum_{i=1}^{n_s}\left[\alpha_{s\phi i}k_{s\phi i}(r_{si}^2 - r_s^2) + k_{s\theta i}\right]$$

and (r_s,ϕ_s) represents the location of the post-yielding stiffness center of the bridge in the $r\phi$-coordinate system defined as [1],

$$r_s = \frac{\sqrt{\left(\sum_{i=1}^{n_s}\alpha_{s\phi i}k_{s\phi i}r_{si}\sin\phi_{si}\right)^2 + \left(\sum_{i=1}^{n_s}\alpha_{s\phi i}k_{s\phi i}r_{si}\cos\phi_{si}\right)^2}}{K_{\Phi}} \quad , \quad \phi_s = \cos^{-1}\left(\frac{\sum_{i=1}^{n_s}\alpha_{s\phi i}k_{s\phi i}r_{si}\cos\phi_{si}}{K_{\Phi}r_s}\right) \tag{10}$$

where $|\phi_s - \pi/2| < \beta/2$. The static radial stiffness eccentricity is defined as $e_{sr0}=r_{s0}-y_m$ in which r_{s0} is the radial coordinate of the pre-yield or static stiffness center ($r_{s0}=r_s$ in Eq. (10) when $\alpha_{sri}=\alpha_{s\phi i}=1$); and, the static azimuthal stiffness eccentricity is defined as $e_{s\phi 0}=\phi_{s0}-\pi/2$ in which ϕ_{s0} is azimuthal coordinate of pre-yield or static stiffness center ($\phi_{s0}=\phi_s$ in Eq. (19) when $\alpha_{sri}=\alpha_{s\phi i}=1$).

iii) $\mathbf{C}$ is damping matrix of the bridge defined based on Rayleigh damping method as follows,

$$\mathbf{C} = \frac{2\xi}{\omega_1 + \omega_3}\left(\omega_1\omega_3\mathbf{M} + \mathbf{K}_0\right) \tag{11}$$

in which $\mathbf{K}_0$ is pre-yield stiffness matrix ($\mathbf{K}_0=\mathbf{K}$ when $\alpha_{sri}=\alpha_{sti}=1$ and i=1,2, …, n_s), ω_1 and ω_3 are natural circular frequencies of the first and third modes computed on the basis of $\mathbf{K}_0$, and ξ is critical damping coefficient assumed to be equal to 2.5%.

iv) $\mathbf{H}_s(t)=\{h_{sx}, h_{sy}, \tau_{s\theta}\}^T$ is total hysteresis force vector of columns in which vector components h_{sx}, h_{sy}, and $\tau_{s\theta}$ are defined as follows,

$$h_{sx} = \sum_{i=1}^{n_s}h_{sri}\cos\phi_{si} - h_{s\phi i}\sin\phi_{si}$$
$$h_{sy} = \sum_{i=1}^{n_s}h_{sri}\sin\phi_{si} + h_{s\phi i}\cos\phi_{si} \tag{12}$$
$$\tau_{s\theta} = \sum_{i=1}^{n_s}h_{s\phi i}r_{si}$$

v) $\mathbf{F}_p(t)=\{f_{px}, f_{py}, t_{p\theta}\}^T$ is total impact force vector in the xy-coordinate system defined as,

$$\mathbf{F}_P(t) = \sum_{i=1,4}\left[\mathbf{N}_{pli}f_{pnli}(t) + \mathbf{T}_{pli}f_{ptli}(t)\right] - \sum_{i=2,3}\left[\mathbf{N}_{pri}f_{pnri}(t) - \mathbf{T}_{pri}f_{ptri}(t)\right] \tag{13}$$

The external force $f_{etaj}(t)$ applied to the deck when the *j*-th contact nodes on the left side (a≡l; j=1, 4) or the right side (a≡r; j=2, 3) sticks (i.e. when $\ddot{\delta}_{ptaj}(t) = \mathbf{T}_{paj}^T\ddot{\mathbf{U}}_o(t) = 0$) is given by [1],

$$f_{etaj}(t) = -\left(\mathbf{T}_{paj}^{T}\mathbf{M}^{-1}\mathbf{T}_{paj}\right)^{-1}\mathbf{T}_{paj}^{T}\left(\mathbf{M}^{-1}\mathbf{C}\dot{\mathbf{U}}_{o}(t) + \mathbf{M}^{-1}\mathbf{K}\mathbf{U}_{o}(t) + \mathbf{M}^{-1}\mathbf{H}_{s}(t) + \mathbf{M}^{-1}\mathbf{F}_{PSj}(t) + \ddot{\mathbf{U}}_{g}(t)\right) \tag{14}$$

where $F_{PSj}(t)$ is defined as [1],

$$\mathbf{F}_{PSj}(t) = \sum_{i=1,4}\left[\mathbf{N}_{pli}f_{pnli}(t) + \mathbf{T}_{pli}(1-\delta_{ij})f_{ptli}(t)\right] - \sum_{i=2,3}\left[\mathbf{N}_{pri}f_{pnri}(t) - \mathbf{T}_{pri}(1-\delta_{ij})f_{ptri}(t)\right] \tag{15}$$

in which δ_{ij} is the Kronecker delta; $\delta_{ij}=1$ when i=j and $\delta_{ij}=0$ when $i \neq j$.

3. Numerical Example

The proposed analytical model is utilized to investigate the seismic responses of a curved bridge prototype subjected to earthquake-induced pounding. Fig. 2 shows geometrical details of this bridge. It is a prestressed reinforced concrete curved bridge consisting of a box-girder deck and four single-column bents. The deck is assumed to be rigid and monolithically connected to the bents. The main geometrical and dynamic parameters of the bridge are [1,26]: β=39.6°, R=305 m, L=210.8 m, M=2894 tons, I_o= 2693×10^8 ton.m^2, υ=20, r_s=300.72 m, y_m=299 m, e_{sr0}=1.72 m, and $e_{s\phi0}$=0 which implies that the bridge stiffness is symmetric with respect to the y-axis, i.e. $\phi_s=\pi/2$.

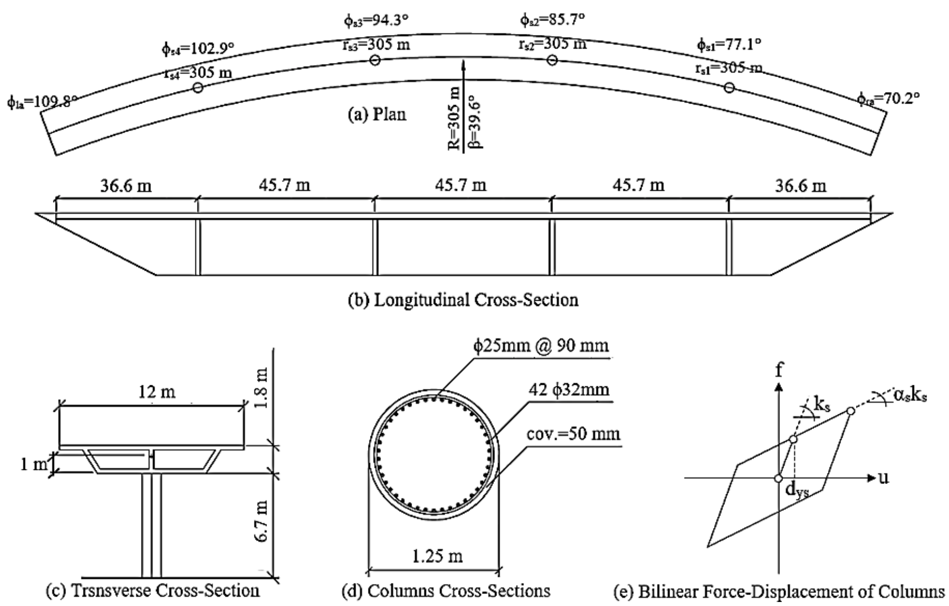

Fig. 2 – Structural details of the curved bridge prototype; (a) plan, (b) longitudinal cross section, (c) transverse cross-section, (d) columns cross-sections, (e) bilinear force-displacement model of columns [1,26].

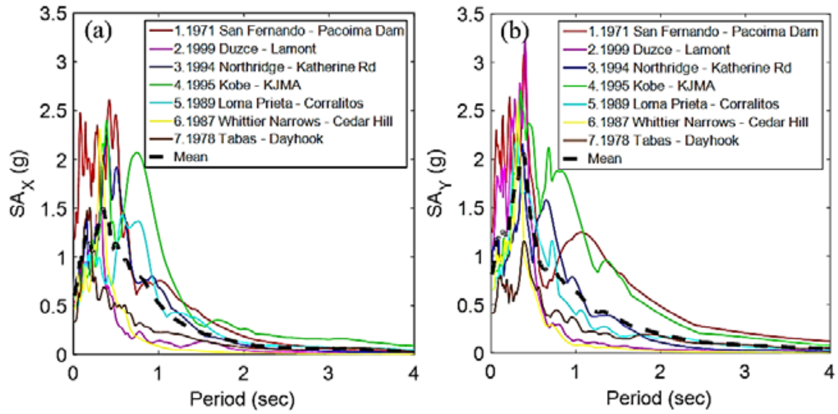

Fig. 3 – Absolute acceleration response spectra of seven pairs of ground motion records applied along the (a) x- and (b) y-axes of the bridge model.

The properties of the bilinear force-displacement behaviors of the columns along the r- and ϕ-axes are shown in Table 1. The dynamic model of the bridge is analyzed under a set of seven ground motion records selected from the PEER Strong Ground Motion Database [27]. Fig. 3 shows the absolute acceleration response spectrums of these ground motions and their geometric mean response spectra along the x- and y-axes. These records have been scaled to a PGA=1.0g representing a very high-intensity ground shaking. The torsional response of the model are taken as the mean of the responses calculated for each principal direction based on the recommendation of AASHTO seismic design guideline [28]. The main parameters of the contact model used in this study are the impact stiffness k_{pn}, the damping ratio ξ_{pn}, the coefficients of static μ_s and kinetic μ_k friction, and the limit velocity of Karnopp friction model v_{s0}. Table 2 presents the values of these parameters obtained from different analytical and empirical methods developed for concrete-to-concrete frictional impacts [1]. The equation of motion (i.e. Eq. (6)) is implemented in *Matlab* and is numerically solved by the 4th-order Runge-Kutta method. In this paper, the size of the time-step is taken to be equal $\Delta t=10^{-3}$ sec, which is not only adequately small to avoid numerical instability and computational error, but large enough to increase the computational speed [1].

Table 1 – Parameters of the bilinear force-displacement behaviors of the columns along the r- and ϕ-axis [1].

Direction	k_s (kN/m)	d_{ys} (cm)	α_s
Radial (r)	16000	8	0.18
Azimuthal (ϕ)	72000	5	0.08

Table 2 – Parameters of the contact model [1].

k_{pn} (N/m$^{1.5}$)	ξ_{pn}	μ_s	μ_k	v_{s0} (m/s)
2.75×10^9	0.35	0.625	0.5	10^{-5}

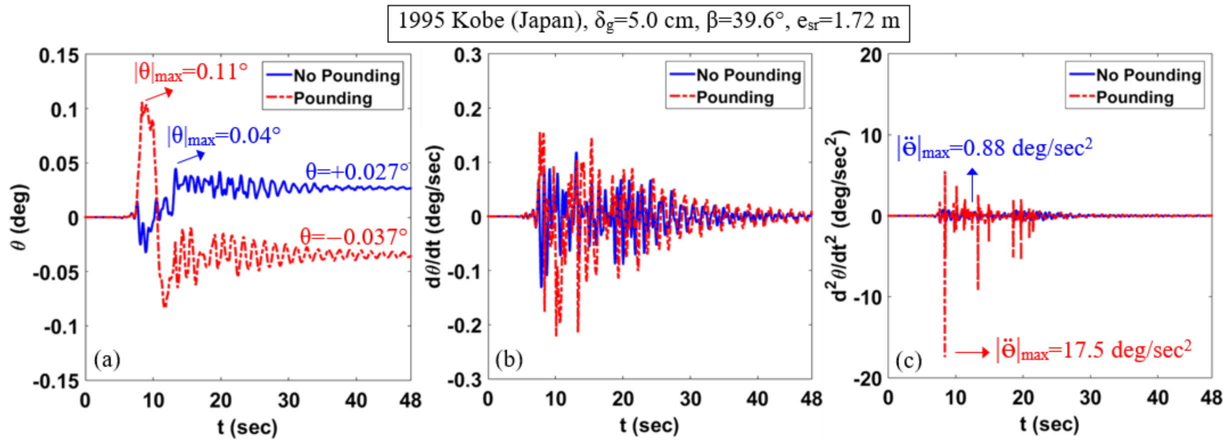

Fig. 4 – Time histories of the torsional responses of the deck for the case of without pounding compared to those of with pounding; (a) rotation, (b) angular velocity, and (c) angular acceleration of the deck.

In order to gain a general insight into the sensitivity of the torsional response of the deck to earthquake-induced pounding, time histories of the rotation, the angular velocity, and the angular acceleration of the curvature center of the deck for the case of pounding are compared to those for the case of without pounding. Figs. 4(a-c) plot these results obtained from the nonlinear time-history analysis of the bridge under the x- and y-components of 1995 Kobe earthquake while it has been assumed that δ_g=5 cm, β=39.6°, and e_{sr0}=1.72 m. It is observed that in contrast to the angular velocity of the deck, the rotation and the angular acceleration of the deck are significantly affected by the seismic pounding. Fig. 4(a) shows that the absolute maximum rotation of the deck is amplified by nearly 3 times from $|\theta|_{max}$=0.04° for the case of no pounding to $|\theta|_{max}$=0.11° for the case of with pounding. The collision between the deck and the abutments results in a permanent clockwise rotation of the deck as much as θ=−0.037° whose magnitude is almost 40% larger than θ=+0.027° for the case of no pounding. It can be seen from Fig. 4(b) that the angular velocity of the deck is not affected so much by the seismic pounding. However, Fig. 4(c) shows that the angular acceleration of the deck is extremely sensitive to the seismic pounding such that it experiences several pulses at the times of the impacts at the contact nodes. The largest one has a magnitude as much as $|\ddot{\theta}|_{max}$=17.5 deg/sec^2 which is 20 times larger than the absolute maximum angular acceleration for the case of no pounding $|\ddot{\theta}|_{max}$=0.88 deg/sec^2. Fig. 5(a-d) show time histories of the normal impact forces at the contact nodes #1, #2, #3, and #4, respectively. As can be seen, the number of impacts between the deck and the left abutment (i.e. impacts at contact nodes #1 and #4) during the earthquake is greater than that for the right abutment (i.e. impacts at contact nodes #2 and #3). Furthermore, the magnitudes of the normal impact forces for the left abutment are higher than those for the right abutment. These impact forces produces a clockwise torsional moment about the curvature center which is the main cause of the permanent clockwise rotation of the deck (θ < 0), as shown in Fig. 4(a).

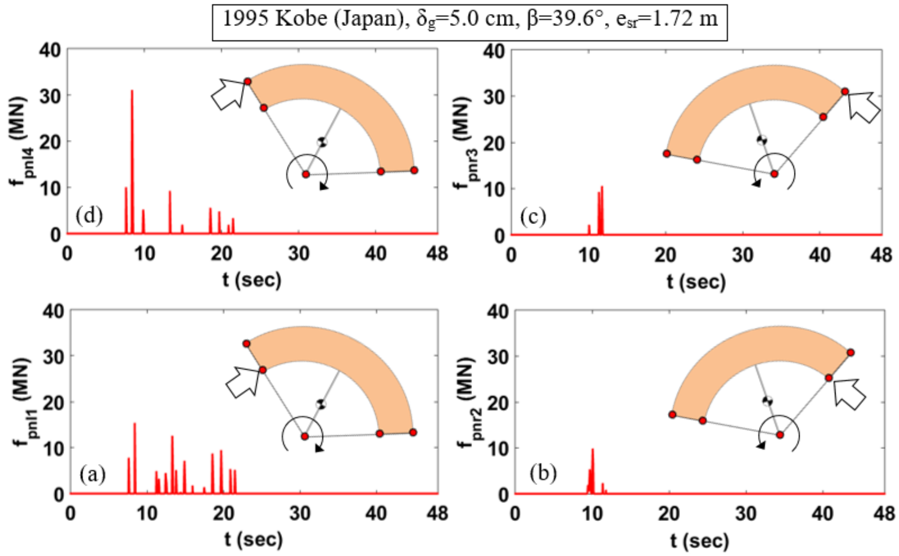

Fig. 5 – Time histories of the normal impact forces at the contact nodes (a) #1, (b) #2, (c) #3, and (d) #4.

4. Parametric Study

The torsional response of horizontally curved bridges subjected to earthquake induced pounding is highly dependent on the parameters of the impact forces, the geometry of the deck, and the stiffness distribution of the columns. In order to identify the key parameters that affect these responses, a detailed parametric study is carried out on the curved bridge prototype by varying different parameters, including the size of the gap between the deck and the abutments, δ_g, from 2.5 cm to 27.5 cm with a step of 2.5 cm, the subtended angle of the deck, β, from 5° to 175° with a step of 17° (note that L is kept constant, L=Rβ=210.8 m, implying that the curved bridges considered with different β are equivalent [28]), and the normalized static radial stiffness eccentricity ratio, $\eta_{sr}=e_{sr0}/r_o$, which can be simplified into following form,

$$\eta_{sr}=\left(\frac{2\nu}{\sqrt{4\nu^2+\beta^2}}\right)\frac{\sum_{i=1}^{n_s}\sin\phi_{si}}{n_s}-\left(\frac{12\nu^2+\beta^2}{3\nu\sqrt{4\nu^2+\beta^2}}\right)\frac{\sin\frac{\beta}{2}}{\beta} \tag{16}$$

It should be noted that the stiffness eccentricity defined here is based on its classical definition, i.e. it is measured from the mass center of the deck. Eq. (16) can be manipulated to vary the location of the stiffness center relative to the mass center which results in three cases: (1) $\eta_{sr}<0$ (asymmetric model, $r_s<y_m$), (2) $\eta_{sr}=0$ (symmetric model, $r_s=y_m$), and (3) $\eta_{sr}>0$ (asymmetric model, $r_s>y_m$). The horizontally curved bridge prototype is analyzed in these three cases in order to investigate the influence of the stiffness eccentricity on the torsional response of the deck. Two extreme arrangements are chosen for the columns on the plane of the bridge in the asymmetric cases of 1 and 3, as shown in Fig. 6 (a) and (c); Fig. 6(b) also shows the arrangement of the columns in the symmetric case, i.e. case 2. Fig. 6(d) shows the variation of η_{sr} with β for these three cases. It is seen that η_{sr} increases with β in cases 1 and 3, but it is zero in case 2 (η_{sr}=0). In order to keep this quantity equal to zero (i.e. to match the location of the stiffness center with that of the mass center) in all values of β considered, the azimuthal coordinates of the columns, ϕ_{si} (i=1, 2, 3, and 4), have to be varied by β according to what shown in Fig. 6(e). The torsional response quantities of interest are the absolute maximums of the rotation and angular acceleration of the deck, i.e. max ($|\theta|$) and max ($|\ddot{\theta}|$), respectively. These response quantities are calculated for each pair of ground acceleration records in Fig. 3 by varying parameters discussed above, and then averaged to calculate the mean response quantities.

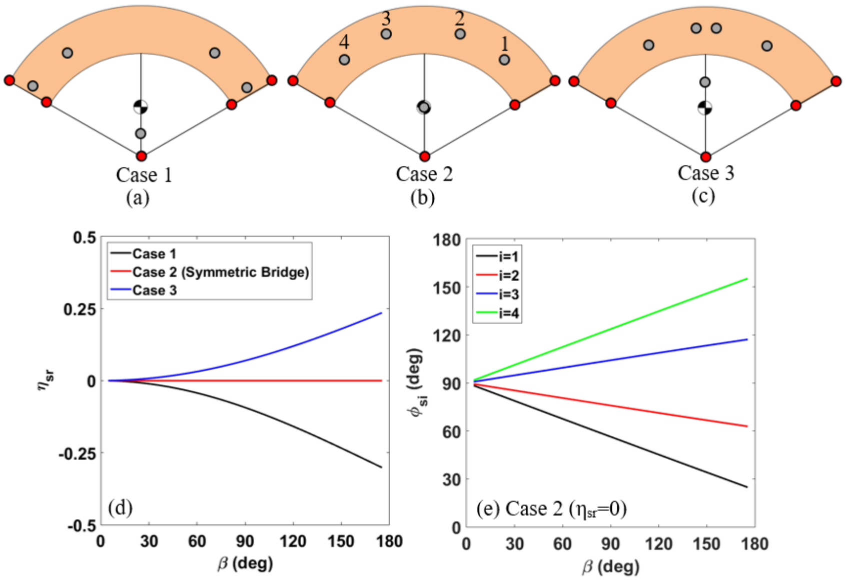

Fig. 6 – (a-c) Sketches of cases 1, 2, and 3 considered for the parametric analysis (d) variation of the normalized static radial stiffness eccentricity ratio, η_{sr}, with β for cases 1, 2, and 3; (e) variation of the azimuthal coordinates of the columns with β for case 2.

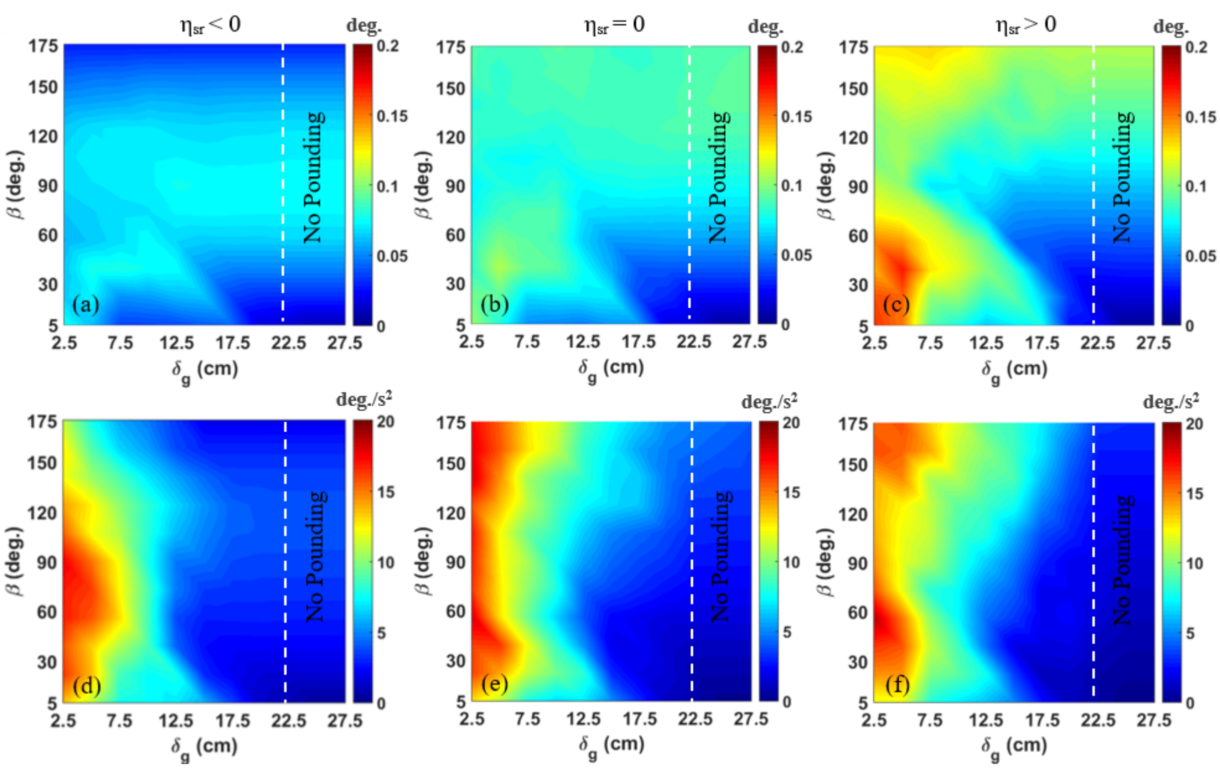

Fig. 7 – Absolute maximum torsional responses of the deck of the curved bridge prototype for different δ_g and β; (a-c) rotation of the deck for cases 1, 2, and 3, respectively; (d-f) angular acceleration of the deck for cases 1, 2, and 3, respectively.

Figs. 7(a)-(c) show 2D image plots of the absolute maximum rotation of the deck versus δ_g and β for cases 1, 2, and 3, respectively. It is seen that for $\delta_g > 22.5$ cm, beyond the dashed lines, the colors of the images do not change with δ_g implying that the seismic pounding does not occur when the size of the gap is larger than 22.5

cm. It is also clear that the rotation of the deck increases with η_{sr} from case 1 to case 3, i.e. when the distance between the stiffness center and the curvature center is increased. The peak value of the rotation of the deck occurs in case 3 and for β and δ_g approximately in intervals 5° < β < 60° and 2.5 cm < δ_g < 7.5 cm, respectively. As the torsional moments of the columns are proportional to the rotation of the deck, $t_{s\theta i} = k_{s\theta i}\theta$, we can expect that the peak of these responses occur at the same values for β and δ_g. Figs. 7(d)-(e) show 2D image plots of the absolute maximum angular acceleration of the deck versus δ_g and β for cases 1, 2, and 3, respectively. It is observed that, in contrast to the rotation of the deck, the angular acceleration of the deck is not very sensitive to the variation in the value of η_{sr}. The variation of this response quantity by δ_g and β has a quite similar trend in the three cases. It can be generally concluded that the peak value of the angular acceleration of the deck in these three cases also occurs for β and δ_g approximately in intervals 5° < β < 90° and 2.5 cm < δ_g < 7.5 cm, respectively.

The results of the parametric analysis show that seismic pounding can significantly amplify the torsional response of the decks of horizontally curved bridges. Therefore, there is a need to protect these bridges from excessive in-plane rotation of the deck under earthquake-induced pounding. For example, seismic protective devices can be useful for this purpose [17,29].

5. Conclusion

In this paper, the sensitivity of the torsional response of horizontally curved bridges subjected to earthquake-induced pounding has been studied by a three-degree-of-freedom nonlinear model. In this model, the radial and azimuthal shear forces of the columns and their bilateral interactions have been modeled by a coupled-biaxial bilinear hysteresis model. The normal and tangential impact forces at the corners of the deck (i.e. contact nodes) have been modeled by Jankowski contact model and the Karnopp friction model, respectively. The bridge model has been employed to analyze the torsional responses of a one-way asymmetric curved bridge prototype ($\phi_s=\pi/2$) to the deck-abutment collisions during strong ground motions. It has been shown that the rotation and the angular acceleration of the deck are more sensitive to seismic pounding than the angular velocity of the deck. Finally, a parametric analysis has been conducted on the curved bridge prototype by varying different parameters of the model, including the size of the gap between the deck and the abutments δ_g, the subtended angle of the deck β, and the normalized static radial stiffness eccentricity η_{sr}. It has been concluded that the rotation of the deck, and consequently, the torsional moments of the columns increase with the increase in the distance between the stiffness center and the curvature center of the deck. The peak value of these responses occur for the curved bridges with 5° < β < 60° and 2.5 cm < δ_g < 7.5 cm when their stiffness centers are located above their mass centers ($\eta_{sr} > 0$).

6. References

[1] Amjadian M, Agrawal AK (2016): Rigid-body motion of horizontally curved bridges subjected to earthquake-induced pounding. *Bridge Engineering*, 10.1061/(ASCE)BE.1943-5592.0000962, 04016090.

[2] Linzell D, Hall D, White D (2004): Historical perspective on horizontally curved I girder bridge design in the United States. *Bridge Engineering*, **9**(3), 218–229.

[3] Kalantari A, Amjadian M (2010): An approximate method for dynamic analysis of skewed highway bridges with continuous rigid deck. *Engineering Structures*, **32**(9), 2850–2860.

[4] Kalantari A, Amjadian M (2010): An approximate method for dynamic analysis of highway skewed bridges with continuous deck. *9th US National and 10th Canadian Conference on Earthquake Engineering 2010, Including Papers from the 4th International Tsunami Symposium vol. 5*, Toronto, Canada.

[5] Amjadian M, Kalantari A, Agrawal AK (2016): Analytical study of the coupled motions of decks in skew bridges with the deck-abutment collision. *Journal of Vibration and Control*, 10.1177/1077546316659781.

[6] Kawashima K (2012): Damage of bridges due to the 2011 great east Japan earthquake. *Proceedings of the International Symposium on Engineering Lessons Learned from the 2011 Great East Japan Earthquake*, Tokyo, Japan.

[7] Jennings PC (1971): Engineering features of the San Fernando earthquake of February 9. *Technical Report California EERL-71-02*, California Institute of Technology Earthquake Engineering Research Laboratory, California, USA.

[8] Bruneau M (1998): Performance of steel bridges during the 1995 Hyogoken–Nanbu (Kobe, Japan) earthquake—a North American perspective. *Engineering Structures*, **20**(12), 1063–1078.

[9] Falamarz-Sheikhabadi MR, Zerva A, Ghafory-Ashtiany M (2016): Mean absolute input energy for in-plane vibrations of multiple-support structures subjected to non-stationary horizontal and rocking components. *Probabilistic Engineering Mechanics*, **45**, 87–101.

[10] Falamarz-Sheikhabadi MR, Ghafory-Ashtiany M (2015). Rotational components in structural loading. *Soil Dynamics and Earthquake Engineering*, **75**, 220–233.

[11] Kawashima K, Takahashi Y, Ge H, Wu Z, Zhang J (2009): Reconnaissance report on damage of bridges in 2008 Wenchuan, China, earthquake. *Earthquake Engineering*, **13**(7), 965–996.

[12] Han Q, Du X, Liu J, Li Z, Li L, Zhao J (2009): Seismic damage of highway bridges during the 2008 Wenchuan earthquake. *Earthquake Engineering and Engineering Vibration*, **8**(2): 263–273.

[13] Sun Z, Wang D, Guo X, Si B, Huo Y (2012): Lessons learned from the damaged Huilan Interchange in the 2008 Wenchuan earthquake. *Bridge Engineering*, **17**(1), 15–24.

[14] Williams D, Godden W (1979): Seismic response of long curved bridge structures: Experimental model studies. *Earthquake Engineering & Structural Dynamics*, **7**(2), 107–128.

[15] Ijima K, Obiya H, Aramaki G, Kawasaki N (2001): A study on preventing the fall of skew and curved bridge decks by using rubber bearings. *Structural Engineering and Mechanics*, **12**(4), 347–362.

[16] Wieser J, Zaghi A, Maragakis M, Buckle I (2012): A Methodology for the experimental evaluation of seismic pounding at seat-type abutments of horizontally curved bridges. *Structures Congress*, Chicago, Illinois.

[17] Ruiz Julian FD, Hayashikawa T, Obata T (2007): Seismic performance of isolated curved steel viaducts equipped with deck unseating prevention cable restrainers. *Constructional Steel Research*, **63**(2), 237–253.

[18] Kalantari A, Amjadian M (2011): Investigation of the seismic pounding effect on torsional response of highway bridges. *6th International Conference of Seismology and Earthquake Engineering*, Tehran, Iran.

[19] Amjadian M, Kalantari A (2012): Influence of seismic pounding on dynamic response of skewed highway bridges. *15th World Conference on Earthquake Engineering*, Lisbon, Portugal.

[20] Mylonakis G, Gazetas G. (2000): Seismic soil-structure interaction beneficial or detrimental? *Earthquake Engineering*, **4**(3), 277–301

[21] Meng JY, Lui EM, Liu Y (2001): Dynamic response of skew highway bridges. *Earthquake Engineering*, **5**(2), 205–223.

[22] Wang CH, Wen YK (2000): Evaluation of Pre-Northridge low-rise steel buildings, I: Modeling. *Structural Engineering*, **126**(10), 1160–1168.

[23] Jankowski R (2005): Non-linear viscoelastic modelling of earthquake-induced structural pounding. *Earthquake Engineering & Structural Dynamics*, **34**(6), 595–611.

[24] Jankowski R (2006): Analytical expression between the impact damping ratio and the coefficient of restitution in the non-linear viscoelastic model of structural pounding. *Earthquake Engineering & Structural Dynamics*, **35**(4), 517–524.

[25] Karnopp D (1985): Computer simulation of stick-slip friction in mechanical dynamic systems. *Dynamic Systems, Measurement, and Control*, **107**(1), 100-103.

[26] Tondini N, Stojadinovic B (2012): Probabilistic seismic demand model for curved reinforced concrete bridges. *Bulletin of Earthquake Engineering*, **10**(5), 1455–1479.

[27] PEER (2013): PEER Ground Motion Database.

[28] AASHTO (2011): Guide Specifications for LRFD Seismic Bridge Design. *American Association of State Highway and Transportation Officials*, Washington, USA.

[29] Agrawal AK, Amjadian M (2016): *Seismic Component Devices*, Innovative Bridge Design Handbook edited by Pipinato A, 1st edition, Butterworth-Heinemann, Boston, 531–553.